A numerical assessment of the scale effects of a ship advancing through restricted waters

Momchil Terziev[1*], Tahsin Tezdogan[1], Atilla Incecik[2]

[1]*University of Strathclyde, Department of Naval Architecture, Ocean and Marine Engineering, Glasgow, UK.*
[2]*University of Strathclyde, Faculty of Engineering, Glasgow, UK.*

**Corresponding author: momchil.terziev@strath.ac.uk*

Abstract

Restricted waters present several challenges for ship builders and operators. The proximity of the seabed and river or canal banks cause viscous effects to be more pronounced than in unrestricted waters. These effects do not follow a linear scaling law, which is typically assumed in terms of sinkage and trim. Moreover, the resistance of the ship is increased in a complex fashion, which has largely eluded researchers. The present study will aim to elucidate scale effects in shallow water performance predictions. Particular attention is placed on the form factor, wave resistance, and frictional resistance. Scale effects are confirmed in the two former parameters. Justification for the obtained results is sought in terms of flow properties. Specifically, the flow velocity and boundary layer thickness are examined in detail. The selected case-study reflects recent experimental work on the KCS hull form in restricted waters.

Keywords: restricted water, RANS, scale effects, KCS, form factor, resistance extrapolation

1. Introduction

Historically, naval architecture has primarily relied on Experimental Fluid Dynamics (EFD) due to the lack of consistently reliable theoretical predictions in the field. The advent of analytical and computational methods has done little in encouraging naval architects to adopt theoretical predictions in their toolkit. Even where this has been the case, computational work usually takes a secondary place. While experimental work has its distinct advantages, the tendency of overreliance on the EFD predictions has some major drawbacks.

Experiments are expensive, especially shallow water cases (Jiang, 2001), they require time, as well as facilities with adequate equipment. Even if all of these requirements are satisfied, one can run into the assumptions of the extrapolation procedures used to determine the full-scale parameters. Specifically, scale effects have been documented in every component of ship resistance (García-Gómez, 2000; Kouh et al., 2009; Raven et al., 2008). Several studies have investigated the impact one's choice of extrapolation procedure on the full-scale resistance of a vessel. For instance, Niklas and Pruszko (2019), Terziev et al. (2019a), and Terziev et al. (2021) found a scatter in results depending on the extrapolation method used.

The case of shallow water presents an additional layer of complexity, because scale effects are expected to be greater than in unrestricted waters (Tuck, 1978). Here, it is important to distinguish between inland ships, which spend their entire operational lives in restricted waters, and seagoing ships. Shallow water studies merit investigation because even seagoing ships enter shallow waters multiple times each voyage. It is precisely in these cases that a significant proportion of accidents occur according to EMSA (European Maritime Safety Agency, 2019, 2018, 2017, 2016, 2015). However, this does not represent the full picture. Inland

transportation will play a major role if carbon dioxide emissions due to transportation are to be reduced. This has led to policies aimed at encouraging the use of navigable rivers and canals (Caris et al., 2014; European Commission, 2018; Mihic et al., 2011).

To facilitate the transition to safer operations in shallow waters, the underlying hydrodynamic phenomena must be better understood. An action taken by the ship in deep water can have counter-intuitive consequences in shallow water (Tuck, 1978). These consequences are caused by the hydrodynamic interaction between the ship's hull and the surrounding bathymetry. Effects include a reduction in under keel clearance which translates into a grounding hazard. Additionally, the resistance is known to increase, and the manoeuvrability characteristics are compromised (Fujino, 1976; Millward, 1996). Faced with the above challenges, many analysis methods are either inapplicable, or perform poorly in shallow water.

The primary goal of this paper is to examine scale effects of the total resistance and its constituent components in confined water. It is important to mention that there have been reports of scale effects in sinkage between model- and full-scale measurements in shallow water (Dand, 1967; Duffy, 2008; Ferguson, 1977; Shevchuk et al., 2019; K. Song et al., 2019). The fact that external parameters, such as wind and waves are impossible to control, as well as the difficulties one faces in full-scale measurements might preclude the identification of the specific root these scale effects experimentally. It may not always be possible to ascertain whether a true scale effect is observed, or if the apparent differences are due to uncontrolled parameters, such as surface roughness, bathymetry irregularity, etc. The adopted case-studies therefore neglect the effects of sinkage and trim.

The lack of experimental data at different scale factors (i.e. a geosim series in a controlled, laboratory environment) for the same ship in confined water motivates a purely numerical study in all but the smallest scale factor, where data is available. The geosim analysis is applied on the well-known KCS hull form, with conditions replicated from recent experimental work, reported in Elsherbiny et al. (2019). To reveal scale effects, double body and multiphase simulations are performed. In the present context, double body simulations refer to the modelling approach where the free surface has been replaced by a symmetry plane. This has the effect of eliminating the wave resistance component from the total resistance. The novelty of this study is expressed in the approaches used to determine the parameters of interest, as well as the adopted case study.

The remainder of this work proceeds with a layout of the necessary background in Section 2, followed by a brief description of the methodology in Section 3, which also contains the ship geometry and case-studies. Section 4 contains the results and relevant discussion, whereas the conclusions and recommendations for future work are laid out in Section 5.

2. Background

A critical part of ship design is to assess the power requirements (Tezdogan et al., 2016b). To obtain a complete picture of a ship's performance, the designer must also understand how the ship will react to a reduction in under keel clearance (Tuck and Taylor, 1970). This may occur whilst entering a port, or traversing one of the famous man-built waterways (the Panama and Suez canals (Tuck, 1966)). It is known that an increase in resistance can be expected when operating in shallow waters. Typically, this is offset by a reduction in speed, also used to insure against groundings, which are the most frequently occurring accidents in the Suez Canal. While

a grounding at low forward speed may not damage the ship from a structural point of view, it creates congestion. The low speed requirement has also meant that the abovementioned waterways have become bottlenecks, restricting the amount of freight passing through. In fact, while the average annual vessel traffic has remained largely constant in the past four decades, freight has increased in an exponential fashion (Suez Canal Authority, 2018). Therefore, ship size must have increased proportionally (Briggs, 2006). This has meant that the main task of the Suez Canal Authority is now to perform bathymetric surveys, since larger vessels require greater under keel clearance and safety margins.

In terms of ship resistance, ship designers have many tools at their disposal. Typically, during the design stage, parameters are predicted in an iterative fashion with ever increasing complexity, culminating in a model experiment. Unfortunately, these are normally confined to unrestricted waters, because shallow water experiments are difficult and expensive (Tuck, 1978), even more so than in deep waters. The implications of this are many. Primarily, the selected resistance extrapolation procedure might only be performed in deep waters.

Extrapolation of ship resistance is performed following the two-dimensional methodology of Froude (1874), or the three-dimensional approach of Hughes (1954). The latter, also known as the form factor approach, is endorsed by the International Towing Tank Conference (ITTC), and is adopted in this study. Both extrapolation procedures begin by decomposing ship resistance into a frictional component and a residual component in the case of Froude's (1874) method, while Hughes (1954) uses wave and three-dimensional effects instead. The frictional resistance is estimated by a friction line or correlation, by calculating the resistance of a flat plate with surface area, equal to the ship's wetted area. A plethora of such relationships (all of which are functions of the Reynolds number) have been developed. Broadly, they are classified as analytical, correlational, or numerical, based on the derivation used in each case. In the present study the frictional resistance data will be compared against 17 such relationships.

One of the most fundamental problems in model tests, and the subsequent extrapolation is that the intrinsic physical properties of the medium (air and water) have not been scaled down along with the ship. In this respect, potential flow can be a useful starting point. Specifically, linear potential flow theories predict no scale effect in the wave pattern, generated by a ship. Therefore, any scale effects stem from the action of viscosity, vorticity, and turbulence. It is this aspect of the physical problem that requires more attention. In this respect, adopting a canal case-study, where both the depth and width are restricted is beneficial. This is because restrictions, whether horizontally or vertically in a seaway are thought to augment the effects of viscosity.

In extrapolation techniques, the running sinkage of the ship is assumed to scale linearly, i.e. with ship length (Gourlay and Tuck, 2001). However, boundary layer physics suggests this should not be the case, because the thickness, and therefore forces within the boundary layer, do not follow the abovementioned scaling law (White, 2010). Here, it is useful to introduce the concept of an "equivalent ship". This is sometimes used in potential flow theories in an attempt to account for boundary layer displacement thickness and its impact on flow properties (Gotman, 2002; Lazauskas, 2009). Simply put, an "equivalent ship" is the ship's underwater geometry, plus the displacement thickness of the boundary layer. Now, the displacement thickness being different at each scale, inevitably means that this equivalent ship operates at

different clearances (from the seabed and/or the canal side – if one exists). That is, even if one is willing to neglect the effects of turbulence and vorticity.

Turbulence and its effects are not well understood on flat plates (Durbin and Pettersson Reif, 2011). Complex shapes, as ships, which feature the free surface effects and strongly three-dimensional boundary layers therefore present an additional difficulty (Magionesi and Di Mascio, 2016). The former have not been accounted for by any turbulence model in their derivation process. In other words, there is doubt and controversy in some aspects of ship hydrodynamics, especially in shallow water cases (Tuck, 1978), where the above effects are more pronounced.

It is well documented that the form factor (1+k) changes with Reynolds number (Re), as demonstrated by many researchers (García-Gómez, 2000; Kouh et al., 2009; Lee et al., 2018; Terziev et al., 2019a; Zeng et al., 2019), but still endorsed as part of the ITTC extrapolation procedure (ITTC, 2017a). The wave resistance is also typically assumed invariant, but as is the case with sinkage and trim, boundary layer physics suggests otherwise. To elaborate, Brard (1970) predicted that viscosity and vorticity act on near-field waves as $1/\left(Re \times F_h^2\right)^{1/3}$, while on far field waves as $1/(Re \times F_h^4)$, where F_h is the depth Froude number and Re is the Reynolds number. Thus, rendering the effect of near-field waves more significant. Coincidently, these are also of greater practical importance in the low speed regime, where the vast majority of ship operate in shallow and/or restricted conditions. This is because ships generate predominantly near-field disturbances at low speeds.

The influence of turbulence is also known to impact on ship-generated waves (Brard, 1970; Tatinclaux, 1970). Since it is not possible to achieve both Reynolds and Froude similarity simultaneously in practice, one retains different flow properties in terms of turbulence and vorticity when extrapolating from model to full-scale. As stated previously, this has the effect of modifying the "equivalent ship" at each scale for the same (depth) Froude number. However, a more subtle consequence manifests itself in the fact that the stern of the ship, which is the second wave maker in terms of importance after the bow, operates in a different flow condition.

One could consider the aforementioned statements from the classical point of view of source strength distribution used by potential flow to model the ship as a wave maker. If boundary layer physics are taken into account, then the source strength, assigned to the stern is not the same at different scales. This is true because the boundary layer is relatively thicker at model scale than at full-scale. Moreover, a higher Reynolds number implies a broadening of the turbulent kinetic energy spectrum (Durbin and Pettersson Reif, 2011). The net effect of this is the presence of eddies of different characteristic length and time scales. All of the above serve to point towards the existence of a viscous effect on the wave resistance, as suggested by Brard (1970) and Tatinclaux (1970).

The arguments laid out so far must also be considered in conjunction with the fact that in each scale factor of a geosim series, the fraction of the ship over which a laminar boundary layer may be observed is different. Furthermore, knowledge that a thickening of the boundary layer occurs with increase in scale factor (decrease in linear dimension) suggests that it may be expected that wave resistance will decrease as one moves up the Reynolds number scale in a geosim series. This was one of the conclusions of Ferguson (1977), who observed this effect experimentally. More recently, studies on ship hull roughness demonstrated that a thicker

boundary layer, resulting from surface roughness decreases wave resistance (S. Song et al., 2019). According to Demirel et al. (2017), the increased viscous effects within the boundary layer of a fouled surface reduce the wave component of resistance by modifying the wave field.

However, Brard (1970) discovered that turbulence and vorticity supress ship waves. Indeed, the presence of turbulence is typically interpreted mathematically as a "sink" for large scale motions (Golbraikh et al., 2013). It is therefore not straightforward to predict whether the wave resistance will be higher or lower *a priori.* This is the case because the combined effect of turbulence, vorticity, and change of boundary layer properties on ship waves are difficult to quantify.

Flow separation is also known to play an important part in model-scale, but not in full-scale (Kouh et al., 2009; Raven et al., 2008). Vortex formation is typically delayed in full-scale, and when it occurs, vortices encounter higher damping than in model-scale (Hochkirch and Mallol, 2000). Both of these effects are likely related to the change in laminar-turbulent boundary layer transition location. This causes the different flow properties generated at each scale to cascade and snowball towards the stern and into the wake itself.

In this work, the deliberate choice is made to examine scale effects in the resistance of a ship advancing through a restricted waterway. In such cases, the level of restriction increases nonlinear and viscous effects. Thus, one might expect to observe pronounced changes in the examined parameters. Sinkage and trim have been shown to vary with scale factor both numerically (Shevchuk et al., 2019; K. Song et al., 2019) and experimentally (Duffy, 2008). More recently, numerical studies on the scale effect of ship squat predicted a deviation between dimensionless sinkage of approximately 5% (Kok et al., 2020). It is therefore justifiable to neglect sinkage and trim to isolate effects on resistance. Maintaining the ship fixed also allows comparison with a recent friction line, designed specifically for the ship used in this study in shallow water conditions under the assumption that the ship has an even keel (Zeng et al., 2019).

Since the inclusion of sinkage and trim would complicate matters significantly their effect is not accounted for, i.e. the ship is kept fixed at all examined scale factors. In fact, their combined effect on the resistance of a ship is of greater relative importance in restricted waters than in infinitely deep and wide waters. Moreover, according to Ferguson (1977), using changes in sinkage and trim as a significant factor in the extrapolation procedure is warranted. Therefore, this is left as a piece of future work.

3. Methodology

This section is split into two major parts. In the first part, the overall procedure and case-studies are presented. The second section contains a description of the numerical set-up used, together with details regarding its implementation.

3.1 Approach to the problem at hand

The approach to the problem adopted herein is to perform a numerical simulation in a single scale factor, where experimental data is available. In particular, the work of Elsherbiny et al. (2019) was selected. For this case, the discretisation uncertainty is estimated to demonstrate the efficacy of the numerical set-up for this case. Specifically, the well-known KCS ship, without appendages was used, in a depth to draught ratio of 2.2 and a depth Froude number (F_h) of 0.303. Although different speeds are also available, as a result of the experiment,

F_h=0.303 was selected as it guarantees a reasonable speed when full-scale is reached (approximately 9 knots). This is chosen to increase the practical relevance of the study.

The choice of the next, higher scale factor (λ) is trivial in the absence of experimental data. For this reason, it was decided to divide λ by 2, followed by a full-scale simulation to arrive at the scale factors and ship properties shown in Table 1. In Table 1, the field labelled as "Dynamic viscosity" is used to reproduce the approach of Haase et al. (2016). In the aforementioned study, the authors devised a procedure whereby a modification of the value of viscosity, a ship may satisfy both Reynolds and Froude similarity simultaneously. The value highlighted in bold is the default used in all simulations, whereas the fields corresponding to the remaining scale factors contain the value used to push the Reynolds number its corresponding value for each λ. This is performed while the linear dimensions are maintained the same. The approach allows one to use a single grid for scale effects assessments.

Recently, the authors used the same approach alongside linear scaling and demonstrated the that the approach provides results that are close to those obtained by a traditional double body simulation (Terziev et al., 2021, 2019a). Around the same time, Sezen and Cakici (2019) performed a similar study, but arrived at the opposite conclusion. This is the case for several reasons. Firstly, in Terziev et al. (2019a), solely double body simulations were performed using the approach referred to as "viscous scaling". This eliminates the issue of viscous effects on the free surface, resulting from the change in the physical properties of the fluid surrounding the ship. However, in the evaluation the performance of the viscous scaling approach, the authors (Sezen and Cakici, 2019) assumed that the residuary coefficient must remain constant. Moreover, the initial methodology of Haase et al. (2016a) validates a grid in model scale, then repeats the simulation with a change in the viscous properties of the fluid. No change in mesh was originally envisioned. Although it is true that the y^+ values cannot remain the same between the different case-studies, a change in mesh characteristics voids the first step, in which validation is performed. In addition, the approach's appeal is expressed in the fact that low cell numbers can be used to perform a full-scale simulation. Reconstructing the mesh and matching the y^+ values negates this appeal as it corresponds to a drastic increase in cell numbers.

Once the viscously scaled simulation has run its course, the results are multiplied by the ratio of scale factors to the third power, thus correcting the discrepancy in linear dimensions.

Table 1. Case-studies

Quantity	Symbol	Value			Unit
Scale Factor	λ	75	37.5	1	-
Length	L	3.067	6.133	230	m
Beam	B	0.429	0.859	32.2	m
Draught	T	0.144	0.288	10.8	m
Depth	D	0.253	0.507	19	m
Water depth	h	0.317	0.634	23.760	m
Block coefficient	C_B	0.651	0.651	0.651	-
Longitudinal Centre of Gravity	LCG	1.488	2.976	111.593	m
Wetted area	S	1.694	6.777	9530	m^2
Speed	U	0.535	0.756	4.630	m/s
Reynolds number	Re	1.840×10^{6}	5.205×10^{6}	1.195×10^{9}	-
Dynamic viscosity	μ	$\mathbf{8.8871\times10^{-4}}$	3.1421×10^{-4}	1.3683×10^{-6}	Pa-s
Depth Froude number	F_h	0.303			-

3.2 Numerical implementation

The placement of the inlet and outlet boundaries follows the recommendations of ITTC (2011) and is shown in Figure 1. The domain top is placed at 1.25×L from the undisturbed water surface, where a velocity inlet condition is imposed. The domain bottom is set to match the experimental condition of h/T=2.2 in all scales, specified as a velocity inlet. Such a boundary condition guarantees that there will be no relative motion between the fluid and the seabed. A velocity inlet may also be preferable due to the fact that open boundaries have a stabilising effect on the numerical solution. In any case, the use of velocity inlets to represent the domain bottom has been validated in recent studies (Elsherbiny et al., 2020). The side boundary is also positioned following the experiment, at 2.3m from the ship centreline in λ=75, and is scaled accordingly. The accompanying mesh for the full-scale multiphase simulation is shown in Figure 2, whereas Table 2 contains the resulting cell numbers for all simulations. It should be noted that the multiphase simulation for λ=75 corresponds to the cell numbers used for viscous scaling.

To ensure that the longitudinal extent of the computational domain does not impact detrimentally the solution, the domain was extended by one ship length on either side of the ship and the simulation repeated. This revealed no discernible change in the results. The near-wall mesh is set to maintain an average of y^+<1 in all model-scale computations, whereas its average value in full-scale is approximately 300. This compromise in altering the y^+ values between model and full-scale is adopted due to the difficulties in modelling a y^+<1 case at full-scale and the coarse nature of the mesh should y^+=300 be adopted at model-scale.

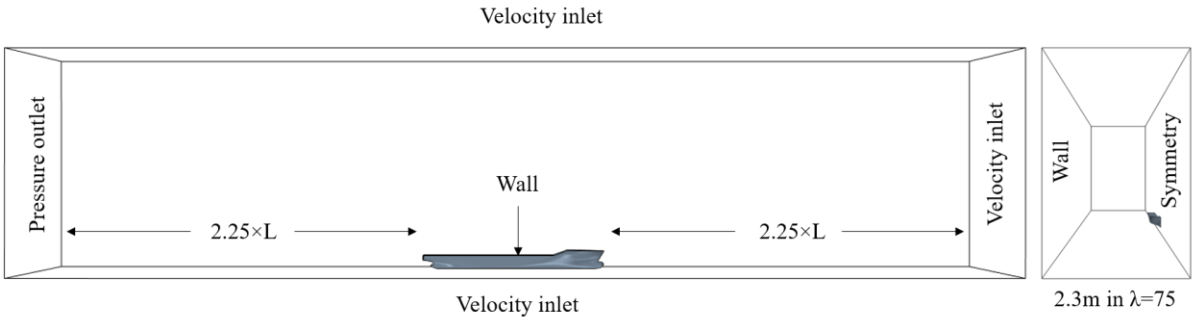

Figure 1. Domain characteristics and boundary conditions

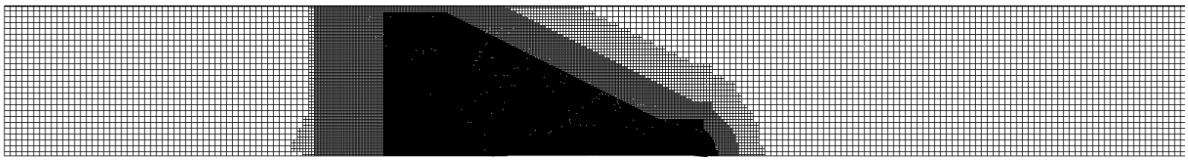

Figure 2. Full-scale mesh generated in Star-CCM+

Table 2. Cell numbers for all simulations.

Scale factor	1	37.5	75
Multiphase	26644375	7938801	4046168
Double body	14339889	2387454	1050032

The simulations which contain both air and water and represent the experimental set-up as accurately as possible are labelled as multiphase. Here, the interphase between the two mediums is modelled by the Volume of Fluid (VOF) method (Hirt and Nichols, 1981). This is a standard approach adopted in the vast majority of marine CFD where the resolution of the free surface is important. The VOF method is also used in Star-CCM+ to model air and water currents and therefore the ship's speed. This is done via the concept of a flat wave, and is set appropriately for each scale, as shown in Table 1. The velocities specified at the inlet boundary, while the outlet is required to maintain the hydrostatic pressure.

To enable the assessment of scale effects, an estimate of the wave resistance and form factor is necessary. In CFD, these can be extracted by performing what is known as a double body simulation. In essence, this is equivalent to replacing the free surface with a symmetry plane. Thus, wave resistance is no longer a component of the total, as shown in Eq. (1a) for multiphase regime, and Eq. (1b) for double body regime:

$$C_T = C_F \times (1+k) + C_W \quad (1a)$$

$$C_T = C_F \times (1+k) \quad (1b)$$

In Eq. (1a) and Eq. (1b), all resistance parameters are shown in non-dimensional form, achieved by division by $0.5 \times S \times U^2 \times \rho$, where S is the wetted area in m^2, U is the ship velocity in m/s, and ρ is the water density (997.561 kg/m^3). To obtain the wave resistance, one must simply subtract the total resistance in double body mode from the multiphase condition, while the form factor (1+k) is obtained by division of C_{Tdb} by C_{Fdb} (Eq. (1a) and Eq. (1b): C_{Tdb}/C_{Fdb}) (Molland et al., 2017), where the *m* subscript refers to multiphase solutions, while *db* indicates double body. It is important to note that CFD predicts ship resistance (C_T) as the sum of normal (pressure resistance C_P – which contains 3D effects (viscous pressure) as well was wave resistance (C_W)), and tangential (frictional resistance C_F) components. It should be noted that

in this paper, flat plate friction lines are not used to determine the form factor as is typically done according to the ITTC (1999). This done in favour of the frictional resistance coefficient obtained from CFD because this matric has been shown to be highly sensitive to ship underwater form as well as depth, rendering the usually used friction lines inapplicable to shallow waters. In other words, the approach of Zeng et al. (2019) is followed.

For the purposes of this study, the standard $k - \omega$ model (Wilcox, 2006) is adopted, as implemented in Star-CCM+ version 13.06.012. Previous work demonstrated the $k - \omega$ model's stability and consistency for the class of problems examined here (Elsherbiny et al., 2020; Terziev et al., 2019b). Moreover, it proved the least computationally expensive two-equation turbulence model. The $k - \omega$ model showed an increase in solution time of 8% compared to a one-equation turbulence model, whereas the $k - \varepsilon$ model increased the wall time by approximately 16%. Due to the high relative importance of turbulent properties, convective and diffusive terms are set to 2nd order.

The temporal evolution of the solution is resolved via a first order implicit unsteady scheme, with a time step (Δt) equal to $\Delta t = 0.0035 \times L/U$. This has been demonstrated to be a good choice in several works, and is adopted here (Terziev et al., 2018). However, it is important to state that any discretisation of the temporal term of the Navier-Stokes equations will inevitably result in some numerical error. These are explored in the following section. The remaining physics, modelled by the incompressible RANS equations, are solved for numerically via the segregated flow solver offered in Star-CCM+. More details can be accessed in Siemens (2018).

4. Results and discussion

4.1 Verification study

As mentioned previously, the first step in the procedure is to determine the uncertainties of the numerical set-up of λ=75. The predicted multiphase total resistance coefficient (5.123×10^{-3}) shows reasonable agreement with the experimental value (5.505×10^{-3}), underpredicting the result by -6.85%. This is thought to be sufficiently accurate, especially considering that in the experiment, the ship was allowed to sink and trim, whereas during the numerical simulation it was kept fixed. The verification study is presented in Table 3 for spatial and Table 4 for temporal discretisation, respectively. It should be noted that the relevant equations and relationships used in the production of Table 3 and Table 4 are omitted. Instead, the reader is referred to the report by the ITTC (2017b). To compute the numerical uncertainty, the Grid Convergence Index (GCI) is used, which is typically treated as the standardised approach to reporting numerical uncertainties.

Table 3 and Table 4 contain the numerical uncertainty estimates induced by the choice if grid and time-step, respectively. The results indicate that the largest uncertainty can be expected from the multiphase RANS simulation (3.348%). In terms of temporal dependence, the simulations do not show significant errors. According to Table 3 and Table 4, the numerical simulations (regardless of physics approach) are more sensitive to grid refinement than they are to a change in the time step.

The choice of refinement ratio is of critical importance in verification studies (Phillips, 2012). This is used as a multiplicative factor to the grid size or time step to coarsen the grid. The choice of $\sqrt{2}$ is chosen in line with the recommendations of the ITTC (2008). In general, the

refinement ratio should be chosen to attain a value between 1.1 and 2, as suggested by ASME (American Society of Mechanical Engineers, 2009).

The grid numbers achieved in this study were as follows. The double body cell numbers for the medium and coarse solution numbered 679,472 and 480,040, respectively. Similarly, the multiphase cell numbers were 2,384,829 and 1,395,411. In the process of coarsening the mesh for the verification study, the properties of the mesh used in defining the surface of the ship have been maintained identical. This is done to preserve an accurate representation of the ship geometry in the process of determining the numerical uncertainty. Such an approach was adopted by Tezdogan et al. (2016b, 2015) and is followed here as well.

The wave resistance coefficient's numerical uncertainty characteristics are also shown in Table 3 and Table 4 for spatial and temporal discretisation, respectively. Here, C_W is calculated as the difference of the multiphase and double body resistance values at each refinement level. In the case of time dependence, the double body simulations exhibit a greater variation in resistance characteristics than the multiphase results. Therefore, C_W is predicted to exhibit an oscillatory behaviour. In this case, the modified relationships, as given in the recent work of Song et al. (2019) are used to predict the uncertainty, since they can cope with oscillations in the data.

The uncertainty estimation technique also requires that other sources of error are small. These include round-off error and iterative error (Ferziger and Peric, 2002). The former is thought negligible in most cases, whereas the latter can have a significant impact. In this work, iterative errors are assessed via the procedure of Roy and Blottner (2006). The results suggest that the smallest iterative errors are found in the case of double body simulations are negligible. On the other hand, the RANS multiphase simulation demonstrated an iterative error of *circa* 0.08%, which is considered sufficiently small. To ensure that the solution has converged, the resistance time-history is monitored alongside the residuals. The former are allowed to decrease by at least three orders of magnitude before the solution is stopped.

Table 3. Spatial discretisation-induced numerical uncertainty (for λ=75). The wave resistance coefficient listed in this table was arrived at by subtracting the double body resistance from the multiphase resistance. The subscripts DB and M stand for double body and multiphase, respectively.

Parameter	Multiphase resistance	Double body resistance	C_w	$(1+k)_{DB}$	$(1+k)_M$
Refinement ratio	$\sqrt{2}$	$\sqrt{2}$	$\sqrt{2}$	$\sqrt{2}$	$\sqrt{2}$
Fine	5.123×10^{-3}	4.752×10^{-3}	0.371×10^{-3}	1.12	1.15
Medium	5.607×10^{-3}	4.745×10^{-3}	0.862×10^{-3}	1.13	1.16
Coarse	6.877×10^{-3}	4.720×10^{-3}	2.157×10^{-3}	1.17	1.19
Convergence	Monotonic	Monotonic	Monotonic	Monotonic	Monotonic
Order of accuracy	2.792	3.377	2.798	3.03	2.14
GCI (%)	3.348	0.020	0.014	0.66	1.32

Table 4. Temporal discretisation-induced numerical uncertainty (for λ=75). The wave resistance coefficient listed in this table was arrived at by subtracting the double body resistance from the multiphase resistance. The subscripts DB and M stand for double body and multiphase, respectively.

Parameter	Multiphase resistance	Double body resistance	C_w	$(1+k)_{DB}$	$(1+k)_M$
Refinement ratio	$\sqrt{2}$	$\sqrt{2}$	$\sqrt{2}$	$\sqrt{2}$	$\sqrt{2}$
Fine	5.123×10^{-3}	4.752×10^{-3}	0.371×10^{-3}	1.12	1.15
Medium	5.215×10^{-3}	4.793×10^{-3}	0.422×10^{-3}	1.13	1.16

Coarse	5.293×10^{-3}	5.010×10^{-3}	0.289×10^{-3}	1.18	1.19
Convergence	Monotonic	Monotonic	Oscillatory	Monotonic	Monotonic
Order of accuracy	2.472	4.79	2.8930	3.27	2.22
GCI (%)	1.109	0.016	0.0012	0.66	1.23

An alternative and more conservative approach to estimate the uncertainty in the wave resistance is to take combine the uncertainties of the multiphase and double body simulations. This can be done by finding the square root of the sum of squares of the two quantities $U_w = \sqrt{GCI_M^2 + GCI_{DB}^2}$, where U_W is the combined uncertainty in the wave resistance, whereas the subscripts M and DB stand for multiphase and double body, respectively. Using this approach, the spatial and temporal discretisation uncertainties in the wave resistance coefficient are approximately 3.35% and 1.11%, respectively. Although tolerable, these values are more than two orders of magnitude greater than the GCI predictions. Therefore, this approach may be better suited to estimating a conservative measure of the wave resistance coefficient's uncertainty.

4.2 Numerical results

In this section, the computed skin friction data are shown for each scale factor according to the three different methods in Figure 3 along some established friction lines. Here, it is evident that the viscous scaling procedure may be used with good accuracy to determine the frictional resistance coefficient. This conclusion may be drawn from the fact that the difference between the linearly scaled multiphase predictions and their viscously scaled counterparts are not substantial. These seem to increase as the Reynolds number approaches its full-scale value, where the viscously scaled simulation predicts the skin friction within 0.1% of the double body result.

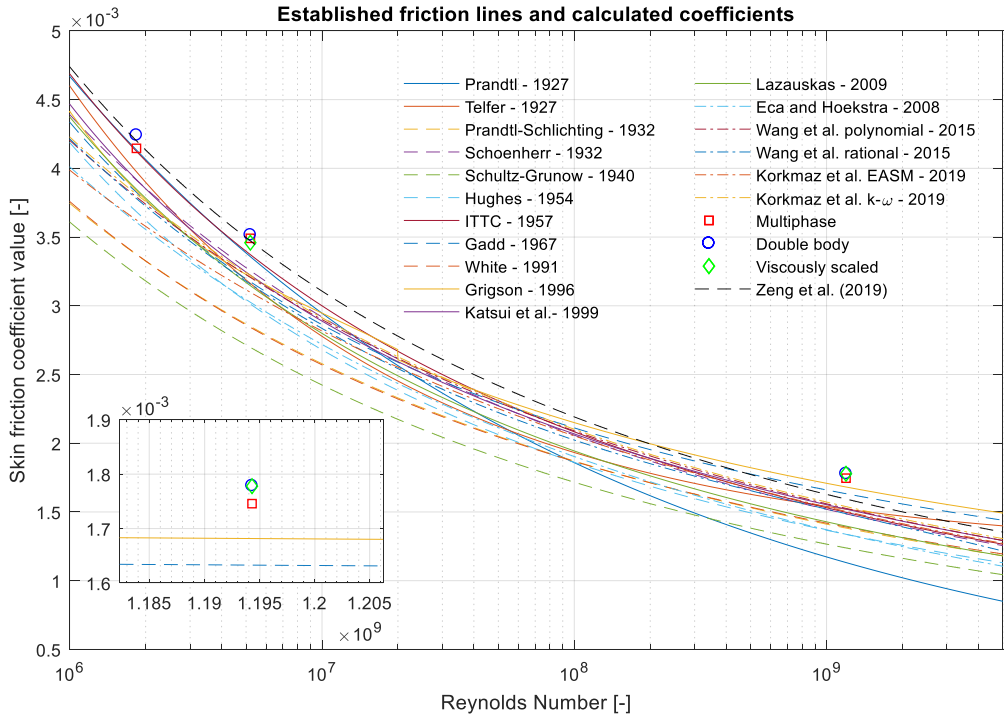

Figure 3. Skin friction coefficients calculated at each scale and established friction lines, used to demonstrate the relative difference between the shallow water line of Zeng et al. (2019) compared to other predictions.

Discrepancies between double body and multiphase results may stem from a variety of sources. These include the small changes of the wetted surface area resulting from the deformation of the free surface. Such effects have been neglected in the present study. Alternatively, research has shown that vortex shedding is modified as a result of the presence of a free surface (Suh et al., 2011). Moreover, such an influence has been documented experimentally by Dand (1967). The same researcher also predicted co-dependence of wave and frictional resistance of a flat plate. Thus, the changes observed in the frictional resistance coefficients are not strictly a manifestation of numerical assumptions.

Now, it is important to put the findings presented in Figure 3 in context and compare the data with other research conducted recently. For this purpose, the friction line, specifically designed for the KCS in shallow water by Zeng et al. (2019) is included alongside the remaining friction lines. One may draw an immediate conclusion that the frictional coefficient is predicted with high accuracy in both model scale factors examined. Indeed, the line of Zeng et al. (2019) outperforms any of the remaining lines in the field. Naturally, this is solely due to the shallow water effect, which is not accounted for in the derivation of any other friction line. However, the full-scale results derived from the present study indicate a problematic trend.

In reaching full-scale Reynolds numbers, the friction line of Zeng et al. (2019) exhibits too great a slope. Thus, the frictional resistance coefficients do not agree well with the data found in this study. Simultaneously, lines with milder slopes, specifically that of Grigson (1999) and Gadd (1967) are closer to the full-scale data. This suggests that at full-scale, the frictional resistance coefficient may be affected by the depth restriction to a lesser extent. The information presented here also points towards the fact that lateral restrictions might not impact the ship resistance significantly in terms of frictional resistance. That is at least at the restriction level posed in this study. However, one may expect that upon reaching significantly more restricted waters, such as narrow canals, the bank effect would be noticeable in the frictional resistance coefficient. In summary, the friction line of Zeng et al. (2019) is shown to perform well in model scale. To determine if the observed discrepancy in full-scale is due to the adopted case study requires further research.

For instance, it may be the case that in full-scale, the effect of the bank is greater than in model scale. To prove or disprove this, analysis is required for different widths, although an attempt at quantifying such an influence is made later in this section. Such assessments do not seem popular in the literature due to the fact that the water depth has a greater bearing on the parameters of interest. One final aspect of the solution that one should consider is the highly specific nature of the friction coefficients and associated line devised by Zeng et al. (2019). The solution included in Figure 3 was generated specifically for the KCS. Indeed, within their work, Zeng et al. (2019) produced lines for two other hull forms. Unfortunately, generalisations to other ships are not possible due to the highly specific nature of the flow in shallow water, which depends heavily on the ship form. This also points to the fact that each underwater shape influences the frictional resistance even in deep waters. Thus, the use of friction lines universally might not be the best approach.

To further support the argument laid out previously, that a free surface modifies the boundary layer, Figure 4 depicts the numerical boundary layer extents in the smallest and largest scale factors. Typically, the extent of the boundary layer is taken as the location where the velocity near a body reaches 99% of its free stream value. In the present case, it was found that such a condition does not lead to a single line, rather, to a small area where the flow attains practically the same speed. For illustration purposes, the boundary layer definition has been slightly altered to 90% of the free stream velocity. This is sampled at four locations, namely, at the forward perpendicular, amidships, at $0.25 \times L_{pp}$ and at the aft perpendicular.

Even after restricting the definition of the boundary layer, it is apparent that amidships the flow velocity near the free surface exhibits several z/L points with the same velocity for a single y/L position. However, it is not thought necessary to restrict the boundary layer definition further as this may impact the resulting data detrimentally. Specifically, the difference in distribution of velocities within the boundary layers of different speeds will reduce as one approaches the solid boundary, where the flow is stationary with respect to the body.

As asserted earlier, all subplots within Figure 4 confirm that at full-scale the boundary layer is thinner than at model-scale. However, the reduction in thickness at the aft perpendicular is seen as the largest. The proximity of the seabed causes the flow to accelerate as the water is passes beneath the ship. Amidships in model scale, connotations of an increasing boundary layer thickness are observed. This phenomenon is predicted by both the free surface and double body method in λ=75. However, the full-scale results exhibit an even weaker vortex, this specific feature being hardly discernible in both multiphase and double body simulations for λ=1. It should be noted that in their recent work, Song et al. (2019) obtained similar results in terms of boundary layer thickness variations in deep waters.

In terms of viscous scaling, it is evident that the method performs adequately. To elaborate, the boundary layer seems to follow the full-scale prediction closely. It is also important to note that in model-scale, the free-surface effect is visible at the forward perpendicular, amidships, and at the aft perpendicular, where the boundary layer broadens as it approaches z/L=0. The same locations are characterised by the absence of the viscously scaled method's boundary layer, in agreement with the full-scale data.

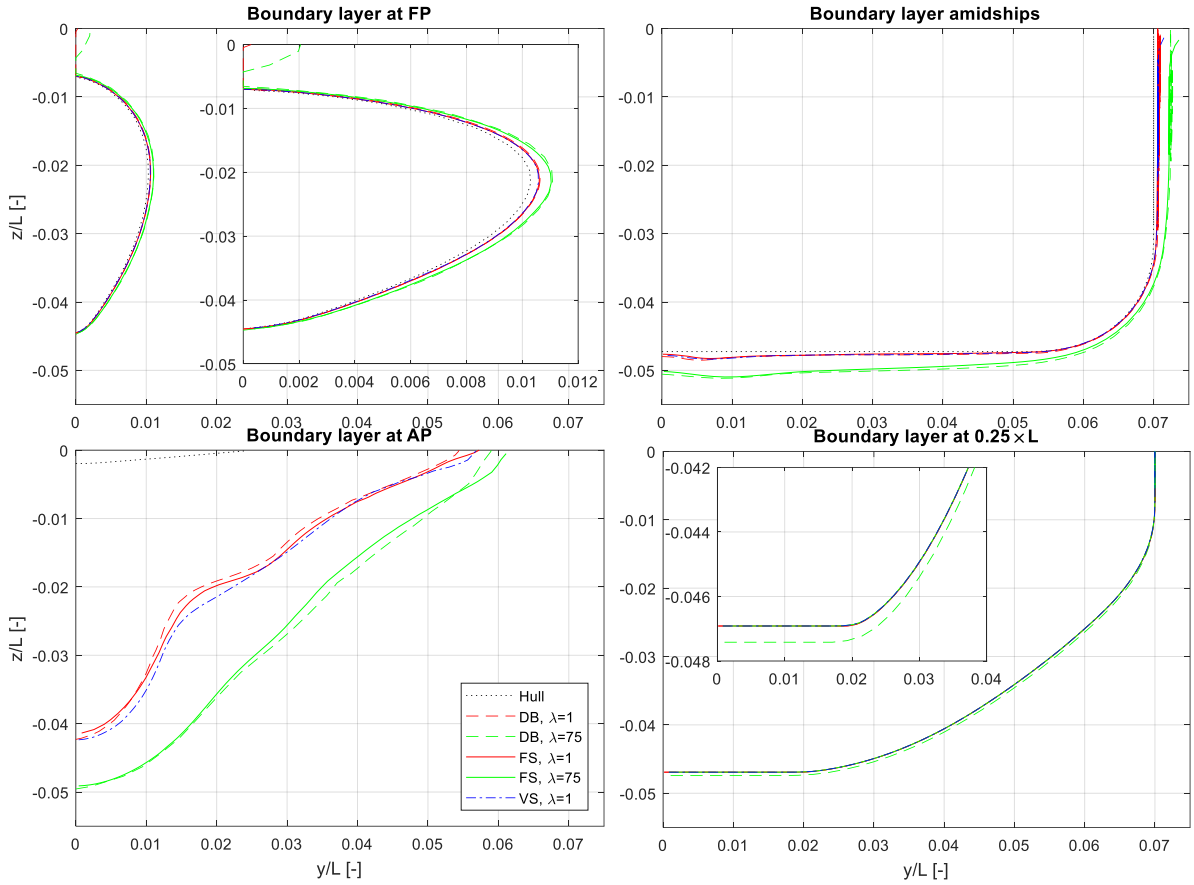

Figure 4. Predicted boundary layer thickness at different scales.

The fact that the viscously scaled predictions model similar behaviour near the free surface is encouraging. However, there is an apparent difference between the frictional resistance coefficients predicted by this method and the linearly scaled simulations. This may stem from a difference in the wetted area, which has been assumed constant (in non-dimensional form) throughout all cases. To further elucidate the potential influence of such an effect, Figure 5 contains the free surface elevations achieved during the course of this study for the largest and smallest scale factors. The intermediate scale has been omitted to allow a clearer depiction of the generated results.

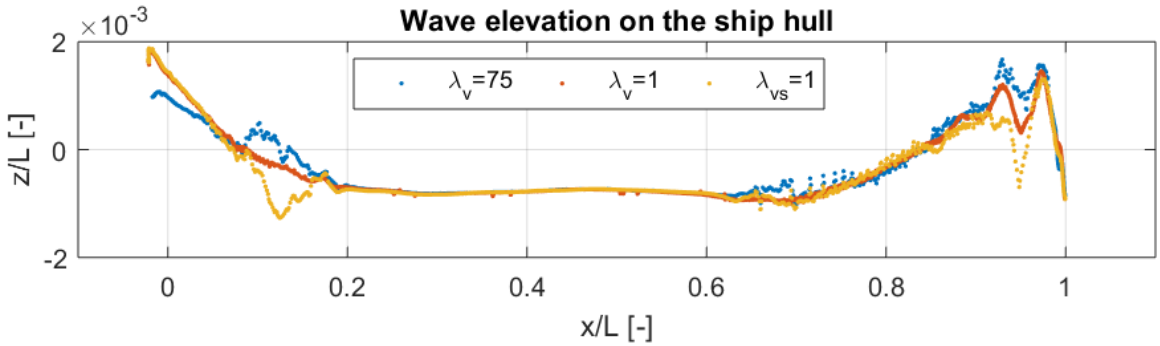

Figure 5. Comparison of the wave elevation on the ship hull.

For consistency, all dimensions have been normalised by the ship length in Figure 5. Here, the result label with a "vs" subscript indicates the viscously scaled result in full-scale. Figure 5 shows that better agreement with the full-scale result is achieved near the stern of the ship via the viscously scaled model, rather than λ=75. Therefore, viscous effects are of lesser consequence in full-scale. This may be deduced by considering the fact that the viscously scaled simulation features a value of viscosity, that is significantly lower than one would normally observe (Table 1 may be consulted for the values).

To provide supporting evidence for the observed phenomena, the reader is directed to the work of Brard (1970) and Tatinclaux (1970), who demonstrated that the action of viscosity, vorticity and turbulence are expected to have an impact on the flow properties. The abovementioned authors studied the effects of viscous, vortical flows on the wave resistance of a ship. Their findings include that a viscous contribution may be identified as part of the wave resistance of a ship.

At this stage, it is worthwhile exploring the reason why potential flow theories do not account for wave elevation changes and the related consequences. According to Brard (1970), vortical and turbulent effects act on the ship in a manner proportional to $1/(Re \times F_h^2)^{1/3}$ in terms of local waves and $1/(Re \times F_h^4)$ in terms of far field waves. Unfortunately, the analysis presented in Brard (1970) is for deep, unrestricted waters. The relative magnitude of the aforementioned terms is shown graphically in Figure 6. However, one may reasonably expect the above effects to be of greater significance in restricted shallow waters. Thus, no logical contradiction is expected when carrying the above relationships to the present analysis. Since the depth Froude number has been maintained constant, it is not though necessary to examine the specific relationships as a function of this particular parameter. Instead, Figure 6 depicts the relative contribution of each wave component (far-field and near-field) with increasing Reynolds number.

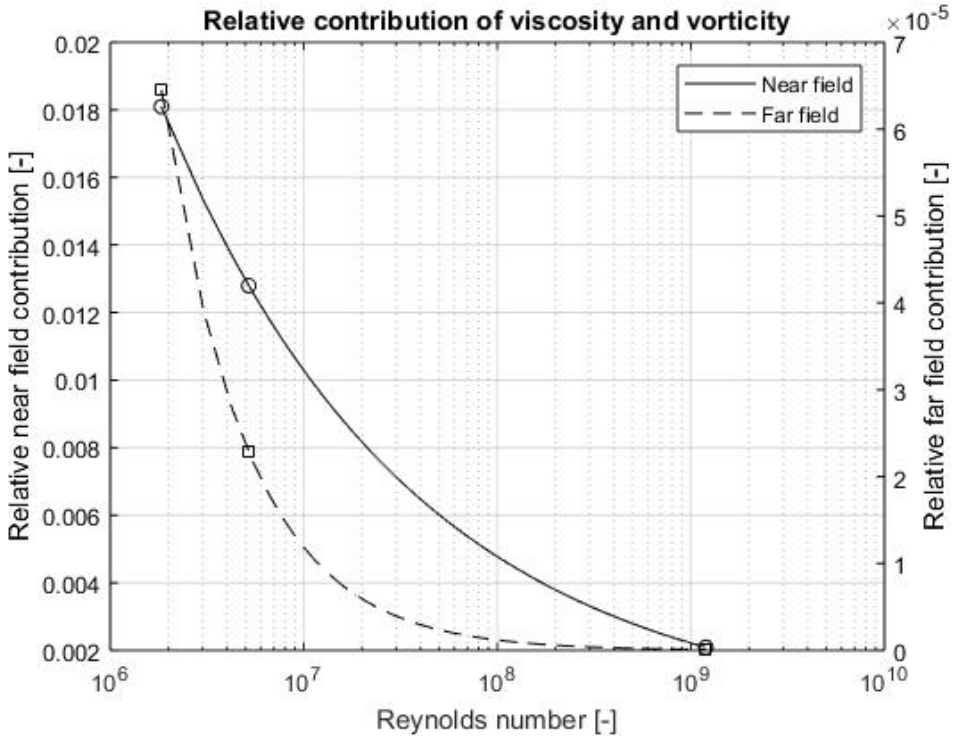

Figure 6. Effect of viscosity and turbulence on near and far field waves according to Brard (1970).

Figure 6 suggests the assertion that viscous effects are of lesser consequence at full-scale in Figure 5 is justified according to the mathematical analysis of Brard (1970). Although the present case studies are restricted to a single speed for which no far field waves are present, it is worthwhile to comment on their potential effect. If a ship propagates at a speed where far field waves are generated, regardless of the water depth and/or restriction, the effect in the far field waves is expected to be greater than that in the near field disturbance. This follows because although the region where viscous effects dominate has become smaller, it has not completely disappeared. Thus, significant proportions of the near field disturbance will be generated and will lie within this region. Conversely, the far field waves will be impacted by a smaller wake, as demonstrated in Figure 4.

As a certain Reynolds number ($\approx 10^7$) is passed, the relative difference between the model and full-scale waves decreases rapidly. This may be confirmed by examination of Figure 6, where it is apparent that the slope of the far field effect is nearly zero for Reynolds numbers past 10^8. A small effect may be expected because the majority of changes in the wake occur in the region Reynolds numbers in the region of $10^6 - 10^7$. Coincidently, this is the region where all model tests are performed due to size limitations. Thus, it may be an inescapable fact that such effects cannot be negated completely by adopting a model with greater linear dimensions. This is also augmented by the fact that as one enters the lower range of Reynolds numbers, both curves increase in magnitude rapidly.

The effects demonstrated in Figure 6 are typically omitted from potential flow theories, even when a nonlinear vortical flow is sought. This is the case because of the small relative magnitude both the near and far field disturbances exhibit, as well as their nonlinear nature. Therefore, an analysis where terms to, say, second order are sought would justifiably not take these terms into account (Brard, 1970; Tatinclaux, 1970).

The next step is to examine the predicted wave resistance. This is shown in Figure 7, using the aforementioned methods (viscous and viscous scaling). The viscously scaled wave resistance coefficient is estimated by subtracting the total resistance as scaled (viscously) and the double body resistance at the specific scale factor.

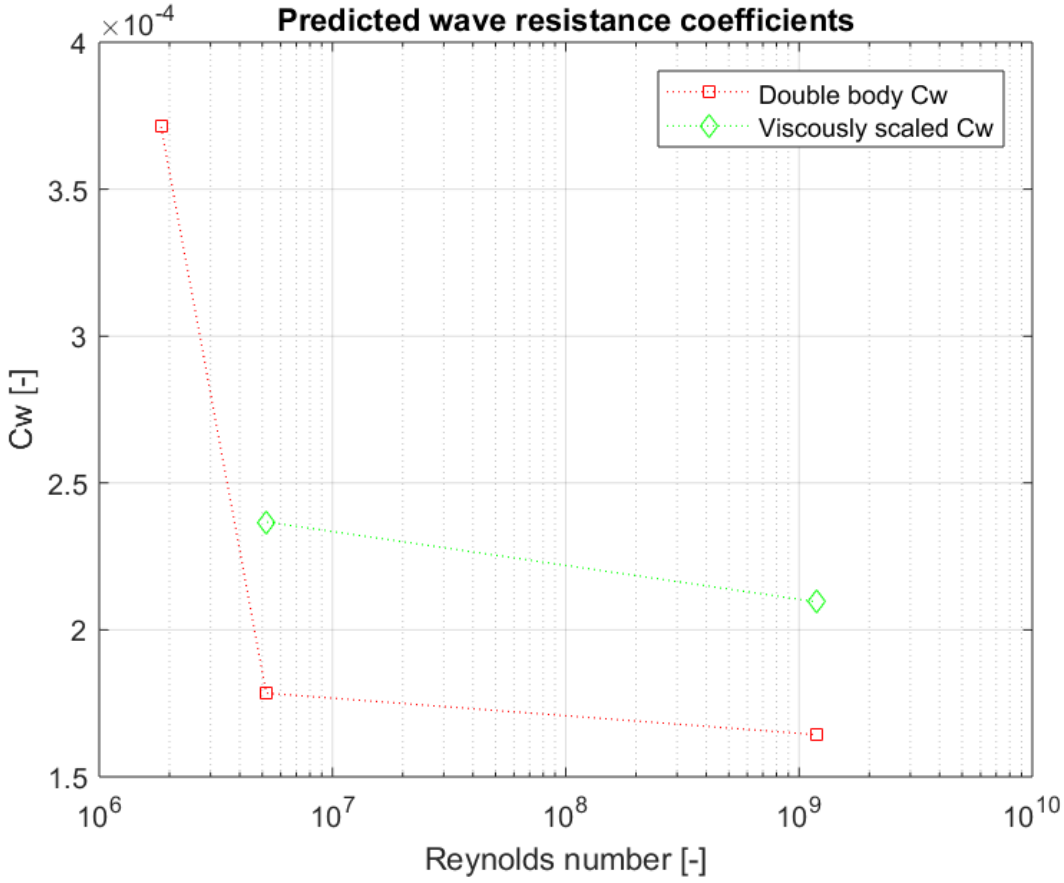

Figure 7. Predicted wave resistance coefficients.

Figure 7 clearly shows that the methods agree in terms of trend – an overall reduction as the scale factor approaches full-scale is observed. Not surprisingly, the predictions follow a pattern closely resembling that of Figure 6, characterised by a sharp decline in the low Reynolds number range, followed by a mild slope. As demonstrated previously, the smallest linear dimensions coincide with those where the viscous effect is expected to be highest. Therefore, the difference between the wave resistance observed at the two adjacent model scale factors is justified. The source of the persistent discrepancy between the methods is likely related to the assumptions in terms of viscosity and double body approximation, although one would expect this to decline further if the Reynolds number were to be increased.

Prior to providing further justification of the results shown thus far, the final set of data is presented. Specifically, Figure 8 depicts the predicted form factors.. The overall trend observed in the figure is that of reduction in (1+k) with higher Reynolds numbers. The best-behaved curve is that calculated via the multiphase method. Indeed, the experimental work of Elsherbiny et al. (2019) suggested the form factor should be in the region of 1.16. The double body prediction seems to resemble this to a lesser extent, and as the scale factor is increased, the data do no decrease monotonically as is the case with the multiphase results.

However, it is not possible to asses scale effects in (1+k) in the absence of experimental data for each scale factor. Moreover, the multiphase method is not characterised by an increase for λ=37.5. This points to the fact that the double body simulation at λ=37.5 may be inaccurate rather than the multiphase one. The change in form factor may be justified by referring to the recent work of Zeng et al. (2019). In the aforementioned work, the authors derived a similar

shape for (1+k). The authors also defined a new relationship for the form factor of the KCS sailing in shallow waters, which is employed in Figure 8.

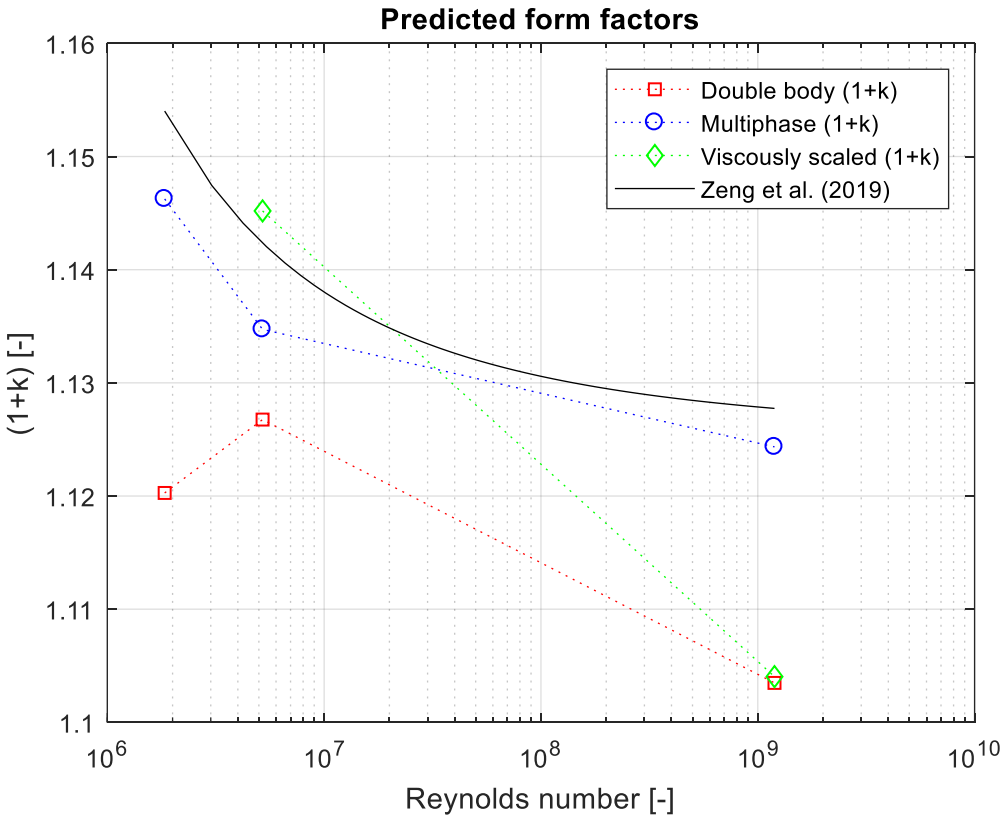

Figure 8. Predicted form factors.

The relationship defining the solid line in Figure 8 due to Zeng et al. (2019) does not take into account the lateral confinement, which is the suspected cause of the observed difference. However, the agreement between the multiphase data and the approximation of Zeng et al. (2019) is seen to be good. Thus, this study confirms the efficacy of the method determined in the previously mentioned reference. Unfortunately, the curve fitting approach used to derive the relationship must be performed anew for each ship. This is because no method is known to determine such an equation for any ship without the presence of data to fit. To prove that the lateral confinement's effect is not as significant as the depth restriction, the velocity distribution along a line in the x –z plane at the aft perpendicular is used. An example of this for [x/L, z/L]=[0, 0.5T] is shown in Figure 9, where the velocity has been normalised by the free-stream velocity. In the present context, this is defined as the flow velocity specified at the inlet. The specific location is chosen in line with the significant difference in boundary layer thickness observed in Figure 4.

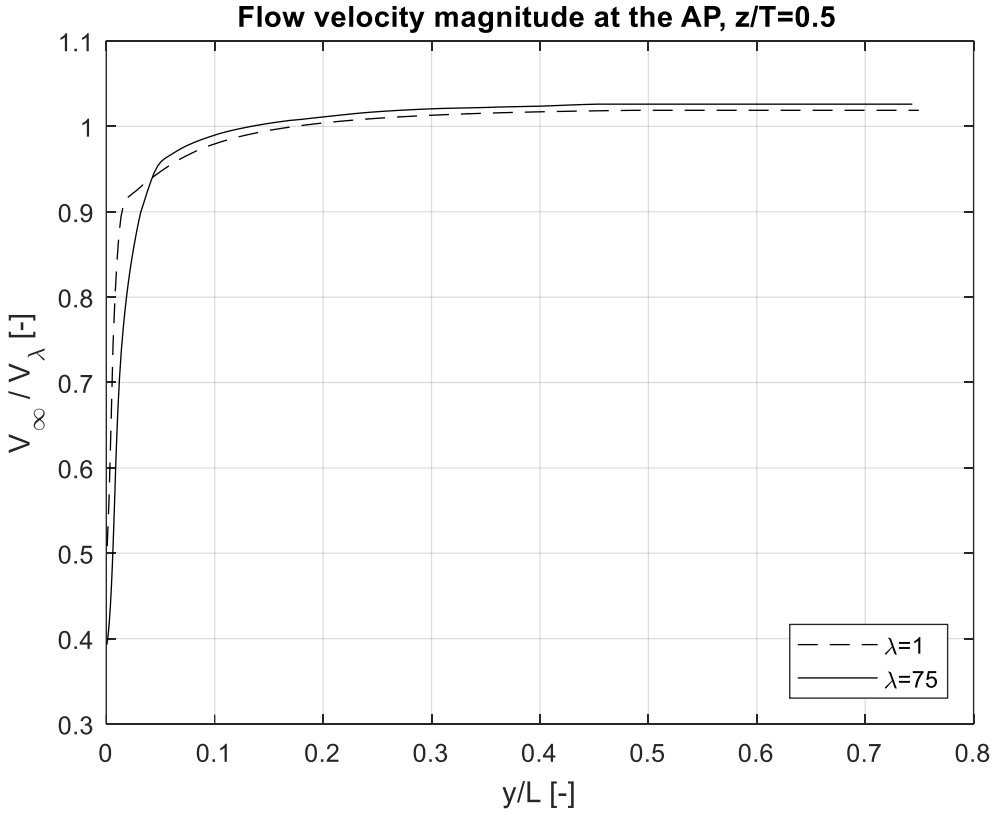

Figure 9. Velocity distribution along a line at the aft perpendicular, z=0.5T. Depicted: multiphase simulations, λ=75 and λ=1.

It is apparent in Figure 9 that the flow is accelerated in a different manner in the two scale factors. More importantly, the flow speed achieved near the tank wall (which is set as a slip wall and therefore does not impact the flow velocity as a no-slip wall would) is higher than the free-stream velocity. In λ=75, the flow velocity is 2.6% higher, whereas in λ=1 – 1.9% higher than that specified at the inlet. In other words, a net difference of 0.7%. Although one may argue that this is not a significant difference, its impact is nonetheless of some, albeit small importance to the ship, particularly on the frictional resistance. The manner in which the different scale factors achieve their maximum flow speeds near the wall is different form one another. Thus, the results from this study can be used to signify that in full-scale, side wall effects are of (slightly) smaller influence than in model scale factors.

Importantly, Figure 9 suggests that flow properties do not scale linearly in highly restricted waterways. Had this been the case, no difference would be present in the curves shown in Figure 9. Therefore, forming a geosim series in such conditions is not as straightforward as simply scaling the tank dimensions. In practice, tanks equipped with false bottoms could be used effectively in this respect. However, if one is to accept the results associated with Figure 9, then the tank dimensions should scale non-linearly. The manner in which this should occur is not known at present, but correction methods similar to Raven (2019) could be considered as a starting point. The issue with such corrections is that they are inherently designed to remove side wall effects, whereas one might wish to maintain this influence when designing, say, a canal boat, or river cruise ship.

The results presented in Figure 9 should also be considered in conjunction with the boundary layer thickness assessment carried out in Figure 4. These jointly suggest that the influence of the water depth scales non-linearly as well as the width. Thus, rendering the possibility of forming a geosim series in shallow water of infinite width equally complex. In fact, the greater proximity of the seabed amplifies the influence of the boundary. Effects of this kind were used as a justification for this study at the onset. It could be considered that these have been proven to a sufficient extent.

The collapsing difference between an infinitely wide water case-study, where the velocity ratio would reach unity, and the canal case explains the discrepancies observed between the present CFD method and the data of Zeng et al. (2019). Specifically, in the low Reynolds number range, the relative difference between the predicted (1+k) and the method of Zeng et al. (2019) is larger than at high Reynolds numbers. This observation fits neatly with the data presented as part of this study. However, it should be kept in mind that a difference of 0.7% falls broadly within the numerical uncertainty predicted for this study. Further studies are necessary to investigate the accuracy of the results observed in this respect.

5. Conclusion

This study has presented a numerical assessment of scale effects of a ship advancing through a canal. To assess the scale effects, a geosim series was formed and evaluated at three different scale factors. The numerical methods used comprise RANS-based multiphase and doubly body simulations. These enabled the assessment of the form factor and wave resistance.

Comparison with recently developed equations describing the frictional resistance revealed excellent agreement with the present CFD set-up in model-scale. For high Reynolds numbers, the large slope of the curve terminated at too low values according to the present CFD method. The aforementioned equations were developed for an infinitely wide shallow water case. Results from this study quantified the influence of the particular canal as small. The flow being accelerated by less than 3% in locations near the wall as a result of the reduced clearance in model scale.

Scale effects on the accelerated velocity were demonstrated in the case of flow near the ship and canal walls. This amounted to 0.7% difference between model and full-scale. In terms of boundary layer, the CFD set-up captured the well-known decrease in thickness. A measurement of the velocity profiles at the aft perpendicular also suggested that the wake volume as a fraction of the ship's displacement is also significantly reduced from model to full-scale.

The predicted form factor showed good agreement with recently established relationships for the KCS. This parameter, along with the wave resistance exhibits a monotonic decline until full-scale. This was confirmed by invoking well-known mathematical analysis which suggests the influence of vorticity and turbulence on the ship decay rapidly with increasing Reynolds number.

This study should be supplemented in several ways. Geosim series with measurements of velocity profiles in the wake, as well as with different surface roughness would be most beneficial. The boundary layer of a rough surface is relatively thicker than that of a smooth surface. Since the decreasing boundary layer with scale is thought to counteract this, it would be interesting to assess this effect in shallow water. Such a study could be conducted along the lines of Song et al. (2019), who performed this for deep, unrestricted waters. However, wave

resistance is of lesser importance in such conditions, which are what could motivate a study in shallow waters.

The effect of sinkage and trim is also of critical importance in shallow water, as well as hull-propeller interactions. Neither of these were incorporated in the present study in the interest of computational savings. In any case, a holistic study, featuring a self-propelled geosim series free to sink and trim in restricted or shallow waters would be most beneficial to the wider field.

Acknowledgements

Results were obtained using the ARCHIE-WeSt High Performance Computer (www.archie-west.ac.uk) based at the University of Strathclyde. The work reported in this paper is drawn from the first author's PhD thesis. The first author gratefully acknowledges the scholarship provided by the Faculty of Engineering at the University of Strathclyde, which fully supported his PhD.

References

ASME (American Society of Mechanical Engineers), 2009. Standard for Verification and Validation in Computational Fluid Dynamics and Heat Transfer - ASME V&V 20-2009, ASME International.

Brard, R., 1970. Viscosity, Wake, and Ship Waves. J. Sh. Res. 14, 1–34.

Briggs, M.J., 2006. Ship squat predictions for ship/tow simulator (ERDC/CHL CHETN-I-72). Erdc/Chl Chetn-I-72 1–18.

Caris, A., Limbourg, S., Macharis, C., van Lier, T., Cools, M., 2014. Integration of inland waterway transport in the intermodal supply chain: A taxonomy of research challenges. J. Transp. Geogr. 41, 126–136. https://doi.org/10.1016/j.jtrangeo.2014.08.022

Dand, W.I., 1967. The wavemaking resistance of ships: Vertical force and form resistance of a hull at uniform velocity. PhD Thesis. University of Glasgow.

Demirel, Y.K., Turan, O., Incecik, A., 2017. Predicting the effect of biofouling on ship resistance using CFD. Appl. Ocean Res. 62, 100–118. https://doi.org/10.1016/j.apor.2016.12.003

Duffy, J., 2008. Modelling of Ship-Bank Interaction and Ship Squat for Ship-Handling Simulation by.

Durbin, P.A., Pettersson Reif, B.A., 2011. Statistical theory and modelling for turbulent flow, Second Edi. ed. Wiley.

Elsherbiny, K., Terziev, M., Tezdogan, T., Incecik, A., Kotb, M., 2020. Numerical and experimental study on hydrodynamic performance of ships advancing through different canals. Ocean Eng. 195. https://doi.org/10.1016/j.oceaneng.2019.106696

Elsherbiny, K., Tezdogan, T., Kotb, M., Incecik, A., Day, S., 2019. Experimental analysis of the squat of ships advancing through the New Suez Canal. Ocean Eng. 178, 331–344. https://doi.org/10.1016/j.oceaneng.2019.02.078

EMSA (European Maritime Safety Agency), 2019. Annual Overview of Marine Casualties and Incidents 2019.

EMSA (European Maritime Safety Agency), 2018. Annual Overview of Marine Casualties and Incidents 2018.

EMSA (European Maritime Safety Agency), 2017. Annual overview of marine casualties and incidents 2017.

EMSA (European Maritime Safety Agency), 2016. Annual overview of marine casualties and incidents 2016.

EMSA (European Maritime Safety Agency), 2015. Annual overview of marine casualties and incidents 2011-2015.

European Commission, 2018. Inland waterways [WWW Document]. Mobil. Transp. URL https://ec.europa.eu/transport/modes/inland_en (accessed 5.17.19).

Ferguson, A.M., 1977. Factors affecting the components of ship resistance. PhD Thesis. University o Glasgow, Department of Naval Architecture. University of Glasgow.

Ferziger, J.H., Peric, M., 2002. Computational Methods for Fluid Dynamics, Springer.

https://doi.org/10.1016/S0898-1221(03)90046-0

Froude, W., 1874. Report to the lords commissioners of the admiralty on experiments for the determination of the frictional resistance of water on a surface, under various conditions, performed at Chelston cross, under the authority of their lordships.

Fujino, M., 1976. Maneuverability in restricted waters, state of the art. National Science Foundation Report No. 184. Department of Naval Architecture and Marine Engineering, College of Engineering, University of Michigan, Ann Arbor, Michigan. Ann Arbor, Michigan.

Gadd, G.E., 1967. A new turbulent friction formulation based on a reappraisal of Hughes' results. Trans. RINA 109, 109–511.

García-Gómez, A., 2000. On the form factor scale effect. Ocean Eng. 27, 97–109. https://doi.org/10.1016/S0029-8018(98)00042-0

Golbraikh, E., Eidelman, A., Soloviev, A., 2013. On helical behavior of turbulence in the ship wake. J. Hydrodyn. 25, 83–90. https://doi.org/10.1016/S1001-6058(13)60341-8

Gotman, A., 2002. Study Of Michell's Integral And Influence Of Viscosity And Ship Hull Form On Wave Resistance. Ocean. Eng. Int. 6, 74–115.

Gourlay, T., Tuck, E.O., 2001. The maximum sinkage of a ship. J. Sh. Res. 45, 50–58.

Grigson, C.W.B., 1999. A planar friction algorithm and its use in analysing hull resistance. Trans. RINA.

Haase, M., Davidson, G., Binns, J., Thomas, G., Bose, N., 2016a. Full-scale resistance prediction in finite waters: A study using computational fluid dynamics simulations, model test experiments and sea trial measurements. Proc. Inst. Mech. Eng. Part M J. Eng. Marit. Environ. 231, 316–328. https://doi.org/10.1177/1475090216642467

Haase, M., Zurcher, K., Davidson, G., Binns, J.R., Thomas, G., Bose, N., 2016b. Novel CFD-based full-scale resistance prediction for large medium-speed catamarans. Ocean Eng. 111, 198–208. https://doi.org/10.1016/j.oceaneng.2015.10.018

Hirt, C.. W., Nichols, B.. D., 1981. Volume of fluid (VOF) method for the dynamics of free boundaries. J. Comput. Phys. 39, 201–225. https://doi.org/10.1016/0021-9991(81)90145-5

Hochkirch, K., Mallol, B., 2000. On the Importance of Full-Scale CFD Simulations for Ships. Numeca 85–95.

Hughes, G., 1954. Friction and form resistance in turbulent flow and a proposed formulation for use in model and ship correlation. Trans. Inst. Nav. Arch. 96.

ITTC, 2017a. Recommended Procedures 1978 ITTC Performance Prediction Method, 4th revision, 7.5 – 02 03 – 01.4. 28th Int Towing Tank Conf.

ITTC, 2017b. ITTC-Recommended Procedures and Guidelines Uncertainty Analysis, Instrument Cali-bration ITTC Quality System Manual Recommended Procedures and Guidelines Procedure.

ITTC, 2011. Recommended Procedures and Guidelines: Practical Guidelines for Ship CFD. 26th Int. Towing Tank Conf.

ITTC, 2008. Uncertainty Analysis in CFD Verification and Validation Methodology and Procedures. 25th ITTC 2008, Resist. Comm. 12.

ITTC, 1999. 1978 ITTC Performance Prediction Method 7.5 - 02 - 03 - 01.4.

Jiang, T., 2001. A New Method For Resistance and Propulsion Prediction of Ship Performance in Shallow Water, in: Proceedings of the Eighth International Symposium on Practical Design of Ships and Other Floating Structures 16 – 21 September 2001 Shanghai, Chaina. pp. 509–515.

Kok, Z., Duffy, J., Chai, S., Jin, Y., Javanmardi, M., 2020. Numerical investigation of scale effect in self-propelled container ship squat. Appl. Ocean Res. 99. https://doi.org/10.1016/j.apor.2020.102143

Kouh, J.S., Chen, Y.J., Chau, S.W., 2009. Numerical study on scale effect of form factor. Ocean Eng. 36, 403–413. https://doi.org/10.1016/j.oceaneng.2009.01.011

Lazauskas, L. V, 2009. Resistance, Wave-Making and Wave-Decay of Thin Ships, with Emphasis on the Effects of Viscosity.

Lee, Y.G., Ha, Y.J., Lee, S.H., Kim, S.H., 2018. A study on the estimation method of the form factor for a full-scale ship. Brodogradnja 69, 71–87. https://doi.org/10.21278/brod69105

Magionesi, F., Di Mascio, A., 2016. Investigation and modelling of the turbulent wall pressure fluctuations on the bulbous bow of a ship. J. Fluids Struct. 67, 219–240. https://doi.org/10.1016/j.jfluidstructs.2016.09.008

Mihic, S., Golusin, M., Mihajlovic, M., 2011. Policy and promotion of sustainable inland waterway transport in Europe - Danube River. Renew. Sustain. Energy Rev. 15, 1801–1809. https://doi.org/10.1016/j.rser.2010.11.033

Millward, A., 1996. A review of the prediction of squat in shallow water. J. Navig. 77–88. https://doi.org/10.1017/S0373463300013126

Molland, A.F., Turnock, S.R., Hudson, D.A., Molland, A.F., Turnock, S.R., Hudson, D.A., 2017. Model–Ship Extrapolation, in: Ship Resistance and Propulsion. Cambridge University Press, Cambridge, pp. 70–85. https://doi.org/10.1017/9781316494196.006

Niklas, K., Pruszko, H., 2019. Full-scale CFD simulations for the determination of ship resistance as a rational, alternative method to towing tank experiments. Ocean Eng. 190, 106435. https://doi.org/10.1016/j.oceaneng.2019.106435

Phillips, T., 2012. Extrapolation-based Discretization Error and Uncertainty Estimation in Computational Fluid Dynamics.

Raven, H.C., 2019. Shallow-water effects in ship model testing and at full scale. Ocean Eng. 189, 106343. https://doi.org/10.1016/j.oceaneng.2019.106343

Raven, H.C., van der Ploeg, A., Starke, A.R., Eca, L., 2008. Towards a CFD-based prediction of ship performance—progress in predicting full-scale resistance and scale effects. Int. J. Marit. Eng. 150.

Roy, C.J., Blottner, F.G., 2006. Review and Assessment of Turbulence Models for Hypersonic Flows: 2D/Asymmetric Cases. 44th AIAA Aerosp. Sci. Meet. Exhib. https://doi.org/10.2514/6.2006-713

Sezen, S., Cakici, F., 2019. Numerical Prediction of Total Resistance Using Full Similarity Technique. China Ocean Eng. 33, 493–502. https://doi.org/10.1007/s13344-019-0047-z

Shevchuk, I., Bottner, C.-U., Kornev, N., 2019. Numerical investigation of scale effects on squat in shallow water, in: 5th MASHCON, Ostend, Belgium. pp. 410–422.

Siemens, 2018. Star-CCM+ User Guide version 13.04.

Song, K., Guo, C., Wang, C., Sun, C., Li, P., Zhong, R., 2019. Experimental and numerical study on the scale effect of stern flap on ship resistance and flow field. Ships Offshore Struct. 0, 1–17. https://doi.org/10.1080/17445302.2019.1697091

Song, S., Demirel, Y.K., Atlar, M., 2019. An investigation into the effect of biofouling on the ship hydrodynamic characteristics using CFD. Ocean Eng. 175, 122–137. https://doi.org/10.1016/j.oceaneng.2019.01.056

Suez Canal Authority, 2018. Suez Canal Traffic Statistics: Annual Report 2018.

Suh, J., Yang, J., Stern, F., 2011. The effect of air-water interface on the vortex shedding from a vertical circular cylinder. J. Fluids Struct. 27, 1–22. https://doi.org/10.1016/j.jfluidstructs.2010.09.001

Tatinclaux, B.J., 1970. Effect of a Rotational Wake on the Wavemaking Resistance of an Ogive. J. Sh. Res. 14, 84–99.

Terziev, M., Tezdogan, T., Demirel, Y.K., Villa, D., Mizzi, S., Incecik, A., 2021. Exploring the effects of speed and scale on a ship's form factor using CFD. Int. J. Nav. Archit. Ocean Eng. 13, 147–162. https://doi.org/10.1016/j.ijnaoe.2020.12.002

Terziev, M., Tezdogan, T., Incecik, A., 2019a. A geosim analysis of ship resistance decomposition and scale effects with the aid of CFD. Appl. Ocean Res. 92. https://doi.org/10.1016/j.apor.2019.101930

Terziev, M., Tezdogan, T., Incecik, A., 2019b. Application of eddy-viscosity turbulence models to problems in ship hydrodynamics. Ships Offshore Struct. 1–24. https://doi.org/10.1080/17445302.2019.1661625

Terziev, M., Tezdogan, T., Oguz, E., Gourlay, T., Demirel, Y.K., Incecik, A., 2018. Numerical investigation of the behaviour and performance of ships advancing through restricted shallow waters. J. Fluids Struct. 76, 185–215. https://doi.org/10.1016/j.jfluidstructs.2017.10.003

Tezdogan, T., Demirel, Y.K., Kellett, P., Khorasanchi, M., Incecik, A., Turan, O., 2015. Full-scale unsteady RANS CFD simulations of ship behaviour and performance in head seas due to slow steaming. Ocean Eng. 97, 186–206. https://doi.org/10.1016/j.oceaneng.2015.01.011

Tezdogan, T., Incecik, A., Turan, O., 2016a. Full-scale unsteady RANS simulations of vertical ship motions in shallow water. Ocean Eng. 123, 131–145. https://doi.org/10.1016/j.oceaneng.2016.06.047

Tezdogan, T., Incecik, A., Turan, O., Kellett, P., 2016b. Assessing the Impact of a Slow Steaming Approach on Reducing the Fuel Consumption of a Containership Advancing in Head Seas. Transp. Res. Procedia 14, 1659–1668. https://doi.org/10.1016/j.trpro.2016.05.131

Tuck, E.O., 1978. Hydrodynamic Problems of Ships in Restricted Waters. Annu. Rev. Fluid Mech. 10, 33–46.

Tuck, E.O., 1966. Shallow-Water Flows Past Slender Bodies. J. Fluid Mech. 26, 81–95. https://doi.org/10.1017/S0022112066001101

Tuck, E.O., Taylor, J.P., 1970. Shallow wave problems in ship hydrodynamics, in: 8th Symposium Naval Hydrodynamics. pp. 627–659.

White, F., 2010. Fluid Mechanics. McGraw-Hill,New York 862. https://doi.org/10.1111/j.1549-8719.2009.00016.x.Mechanobiology

Wilcox, D.C., 2006. Turbulence modeling for CFD, 3rd ed, Transportation Research Record. DCW Industries. https://doi.org/10.1016/j.aqpro.2013.07.003

Zeng, Q., Hekkenberg, R., Thill, C., 2019. On the viscous resistance of ships sailing in shallow water. Ocean Eng. 190, 106434. https://doi.org/10.1016/j.oceaneng.2019.106434